PHYSICAL REVIEW B VOLUME 15, NUMBER 1 1 JANUARY 1977

Neutron scattering study of the lattice dynamics of AgBr at 4.4 K

Y. Fujii, S. Hoshino, S. Sakuragi, and H. Kanzaki
Institute for Solid State Physics, The University of Tokyo, Roppongi, Minato-ku, Tokyo 106, Japan

J. W. Lynn* and G. Shirane
Brookhaven National Laboratory,† Upton, New York 11973
(Received 26 July 1976)

The phonon dispersion relations of AgBr at 4.4 K have been measured in the three principal symmetry directions using the triple-axis neutron scattering technique. The data have been fitted by the extended shell model developed by Cochran *et al.* and the one-phonon density of states has been calculated. Near the zone boundary in the [111] direction (L point), high-resolution measurements of the TA and TO phonon intensities have been carried out. The character inversion between these two modes at L originally predicted by Fischer *et al.* is clearly evidenced from the observed intensities. The present model fit can also reproduce this character inversion. Infrared absorption and luminescence spectra of AgBr have been remeasured at 2 K with high resolution and low concentration of impurities. The observed spectral shape of the one-phonon sidebands can be successfully analyzed using the one-phonon density of states obtained at 4.4 K in the present study.

I. INTRODUCTION

For many years there has been considerable interest in the basic properties of silver halides, AgBr and AgCl. Experimental studies by Brown and his collaborators,[1] together with theoretical calculations[2] have clarified the band structure of the silver halides through experiments on fundamental absorption and photoexcited carriers.[3] Recently, information on trapping and recombination of carriers has been obtained by Kanzaki and Sakuragi through photoluminescence and transient absorption experiments.[4,5] However, information on the lattice-dynamical properties of these compounds has been unavailable until recently, and this has prevented a detailed analysis of many electronic and optical phenomena in the silver halides in which electron-phonon interactions are important. The situation was in contrast with alkali halides, on which extensive lattice-dynamical studies have been made both experimentally and theoretically.

In 1970, inelastic neutron scattering experiments on AgCl were carried out by Vijayaraghaven *et al.*[6] They analyzed the observed phonon dispersion relations using an extended-shell model developed by Cochran *et al.*[7] The experimental success was followed by a theoretical investigation of the lattice-dynamical properties of the silver halides. Fischer *et al.*[8] introduced a new deformable-shell model in which both a quadrupolar deformability and a rigid rotation of the Ag^+ shell were taken into account, and were able to successfully analyze the AgCl data. Furthermore, for AgBr they predicted the character inversion between the TA and TO phonon modes at the L point, the zone boundary in the [111] direction in reciprocal space. This character inversion is crucial to understanding the phonon-assisted indirect band-gap transitions. Neutron scattering experiments on AgBr at 4.4 K by Kanzaki *et al.*[9] confirmed this character inversion experimentally and also led to the conclusion that the valence-band maximum is located exactly at the L point. von der Osten and Dorner[10] independently carried out a neutron scattering experiment at 85 K and reported a similar result. During the course of the present work, Bührer[11] reported the measurements of phonon dispersion curves at 80 and 295 K independently. He analyzed his data by the slightly modified deformable-shell model of Fischer *et al.*[8] and succeeded in reproducing the character inversion at the L point. Recently, Dorner *et al.*[12] extended the previous phonon measurements at 85 K by von der Osten and Dorner.[10] Their deformable-shell-model analysis of the data (85 K) gave similar results to those by Bührer[11] (80 K).

One of the purposes of the present study is to give a full account of our previous measurements briefly reported[9] and to clarify the unique lattice-dynamical properties of the silver halides. In this respect, phonon dispersion measurements near liquid-helium temperature are desirable because of the anharmonic behavior of this crystal.[13] The other is the assignment of phonons responsible for the one-phonon satellite bands associated with the transitions due to localized electronic states in AgBr. Observation of well-resolved phonon sidebands in various optical spectra[4,5] is one of the interesting features of AgBr, partly because of weaker electron-phonon interactions compared with alkali halides, for example. For this purpose, the neutron scattering study at 4.4 K is de-

sirable in comparing the one-phonon density of states with the sharp optical spectra which can usually be observed only at low temperatures.

II. EXPERIMENTAL DETAILS

A spherical single crystal of AgBr was grown by the Bridgman method. The sample tube of fused quartz used for the crystal growth is shown in Fig. 1. The slowly tapered part below the spherical bulb is instrumental in producing a high-quality single crystal. Otherwise, the procedure of sample preparation was the same as reported previously.[4] Crystallization from the melt was carried out in high vacuum at the growth speed of 3 mm/h. After solidification, the sample ingot was taken out by breaking the container and the extra part was removed by a string saw using KCN solution. After polishing, the sample was annealed at 390 °C and then slowly cooled to room temperature.

The sample was made approximately spherical in shape (12 mm in diameter) for the present neutron scattering experiments in order to avoid shape effects due to the appreciable absorption by Ag. The sample was wrapped in a thin Teflon sheet to prevent any chemical reactions with the sample container and was placed in a spherical capsule made of aluminum. Sheets of aluminum foil were wrapped around the sample to provide a tight fit and maintain good thermal contact. The capsule was placed in an aluminum can filled with He gas and mounted in a variable-temperature cryostat with the ⟨100⟩, ⟨110⟩, or ⟨112⟩ axes vertical depending upon experimental requirements. The measurements in the present experiment were carried out at 4.4 K. The sample mosaic was measured to be 18 min [full width at half-maximum (FWHM)].

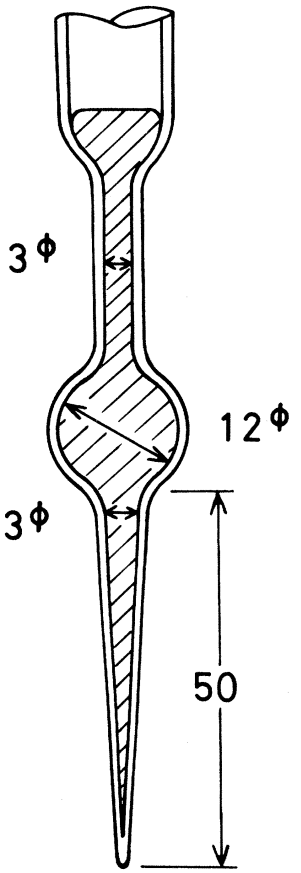

FIG. 1. Cross-sectional view of the sample tube used for growth of the spherical AgBr single crystal. The numerical values represent the tube size in units of mm (ϕ: diameter).

Measurements of the phonon energies were performed with triple-axis neutron spectrometers at the Brookhaven High Flux Beam Reactor. Fixed incident neutron energies of 5.0, 14.8, and 44.0 meV or fixed scattered neutron energies of 14.8 and 24.0 meV were used at various stages of the experiment. Monochromator and analyzer crystals were pyrolytic graphite with 30-min mosaic; the former was vertically bent while the latter was planar. Horizontal collimations (inpile, monochromator-sample, sample-analyzer, and analyzer-detector) were 20 or 40 min depending upon the resolution and intensity needs. Higher-order contamination of the incident neutron beam was suppressed by use of a graphite filter. The spectrometers were operated in the constant-Q mode. Some phonons were measured with several different instrumental conditions to ascertain the reproducibility and reliability of the results.

Each phonon intensity profile measured in the constant-Q scans was least-squares fitted to the sum of a Gaussian function and a linearly varying background. The position of the Gaussian then determined the nominal phonon energy in the scan.

III. EXPERIMENTAL RESULTS

Phonon energies measured at 4.4 K along the three symmetry directions are displayed in Table I. The errors were evaluated from the reproducibility of the results around different reciprocal-lattice points and under different instrumental conditions and are considered to reflect two standard deviations. Wave vectors q are given in terms of the reduced unit ζ, where $\zeta = q(a/2\pi)$ and a is the measured lattice constant (at 4.4 K, $a = 5.730 \pm 0.003$ Å). In this paper, the subscripts 1 and 2 which distinguish between the two transverse modes propagating along the $[\zeta\zeta 0]$ direction (for example, TA_1 or TO_2 in Table I) correspond

to their polarization vectors parallel to the [$\bar{1}$10] and [001] directions, respectively. The data given in Table I are plotted in Fig. 2. The uncertainties are shown by the vertical bars when they are more than the size of plotted symbols.

Special attention was given to a precise intensity measurement of the TA and TO phonon modes near the L point, $\vec{q}=(\frac{1}{2},\frac{1}{2},\frac{1}{2})$. Although our previous measurement[9] was sufficient to confirm the occurrence of the character inversion between these two modes at the L point, the energy resolution [2.5 meV (FWHM)] was not sufficient to clearly separate the two peaks. Measurements with resolution sufficient to separate them are difficult for three reasons; (i) the relatively high absorption by Ag; (ii) the small thermal occupation for phonon states at this temperature (4.4 K); and (iii) no instrumental "focusing" condition for these zone-boundary phonons. In the higher-resolution measurements, we employed a scattered neutron energy of 14.8 meV and the collimation of all 40 min. This gives an energy resolu-

TABLE I. Phonon energies of AgBr at 4.4 K (in meV).

		[ζ00]		
ζ	TA (Δ_5)	LA (Δ_1)	TO (Δ_5)	LO (Δ_1)
0 (Γ)	···	···	10.69 ± 0.32	17.24 ± 0.52
0.05	···	1.15 ± 0.03	···	···
0.10	0.90 ± 0.03	2.29 ± 0.07	10.59 ± 0.32	16.97 ± 0.51
0.15	···	3.52 ± 0.11	···	···
0.20	1.64 ± 0.05	4.70 ± 0.14	10.97 ± 0.33	16.18 ± 0.49
0.30	2.26 ± 0.07	6.81 ± 0.20	11.25 ± 0.34	15.60 ± 0.47
0.40	2.78 ± 0.08	8.67 ± 0.26	11.58 ± 0.35	14.77 ± 0.44
0.50	3.14 ± 0.09	9.61 ± 0.29	12.21 ± 0.37	14.24 ± 0.43
0.60	3.41 ± 0.10	9.56 ± 0.29	12.59 ± 0.38	14.33 ± 0.43
0.70	···	8.72 ± 0.26	13.16 ± 0.39	14.98 ± 0.45
0.80	3.82 ± 0.11	7.29 ± 0.22	13.55 ± 0.41	16.00 ± 0.48
0.90	···	6.08 ± 0.18	13.85 ± 0.42	16.97 ± 0.51
1.00 (X)	3.87 ± 0.12	5.66 ± 0.17	14.16 ± 0.42	17.20 ± 0.52
		[$\zeta\zeta\zeta$]		
ζ	TA (Λ_3)	LA (Λ_1)	TO (Λ_3)	LO (Λ_1)
0.05	0.96 ± 0.03	1.93 ± 0.06	11.00 ± 0.33	···
0.075	1.44 ± 0.04	···	···	···
0.10	1.86 ± 0.06	3.74 ± 0.11	10.60 ± 0.32	17.27 ± 0.52
0.15	2.88 ± 0.09	5.48 ± 0.16	···	···
0.20	3.60 ± 0.11	7.21 ± 0.22	10.19 ± 0.31	17.01 ± 0.51
0.25	4.37 ± 0.13	8.63 ± 0.26	···	···
0.30	4.99 ± 0.15	9.75 ± 0.29	9.41 ± 0.28	16.79 ± 0.50
0.35	5.58 ± 0.17	10.72 ± 0.32	···	···
0.40	6.03 ± 0.18	11.41 ± 0.34	8.61 ± 0.26	16.68 ± 0.50
0.45	6.34 ± 0.10	11.96 ± 0.36	8.15 ± 0.10	···
0.50 (L)	6.68 ± 0.10	12.00 ± 0.30	7.99 ± 0.10	16.51 ± 0.50

			[$\zeta\zeta$0]			
ζ	TA_1 (Σ_4)	TA_2 (Σ_3)	LA (Σ_1)	TO_1 (Σ_4)	TO_2 (Σ_3)	LO (Σ_1)
0.10	1.77 ± 0.05	1.12 ± 0.03	3.16 ± 0.09	10.47 ± 0.31	10.73 ± 0.32	···
0.15	2.56 ± 0.08	1.67 ± 0.05	4.62 ± 0.14	···	···	···
0.20	3.36 ± 0.10	2.22 ± 0.07	6.11 ± 0.18	9.74 ± 0.29	11.33 ± 0.34	16.72 ± 0.50
0.25	4.09 ± 0.12	···	···	···	···	···
0.30	4.77 ± 0.14	3.02 ± 0.09	8.42 ± 0.25	8.96 ± 0.27	12.08 ± 0.36	···
0.35	5.42 ± 0.16	···	···	···	···	···
0.40	6.03 ± 0.18	3.78 ± 0.11	9.76 ± 0.29	8.07 ± 0.24	12.73 ± 0.38	15.72 ± 0.47
0.50	6.85 ± 0.21	4.40 ± 0.13	10.78 ± 0.32	8.34 ± 0.25	13.84 ± 0.42	15.31 ± 0.46
0.60	6.18 ± 0.19	4.71 ± 0.14	10.08 ± 0.30	9.72 ± 0.29	14.71 ± 0.44	15.02 ± 0.45
0.70	5.49 ± 0.16	5.17 ± 0.16	9.02 ± 0.27	11.34 ± 0.34	15.68 ± 0.47	14.64 ± 0.44
0.80	4.71 ± 0.14	5.41 ± 0.16	7.03 ± 0.21	12.74 ± 0.38	16.37 ± 0.49	14.69 ± 0.44
0.90	3.99 ± 0.12	5.59 ± 0.17	4.79 ± 0.14	13.61 ± 0.41	16.78 ± 0.50	···
1.00 (X)	3.87 ± 0.12	5.66 ± 0.17	3.87 ± 0.12	14.16 ± 0.42	17.20 ± 0.52	14.16 ± 0.42

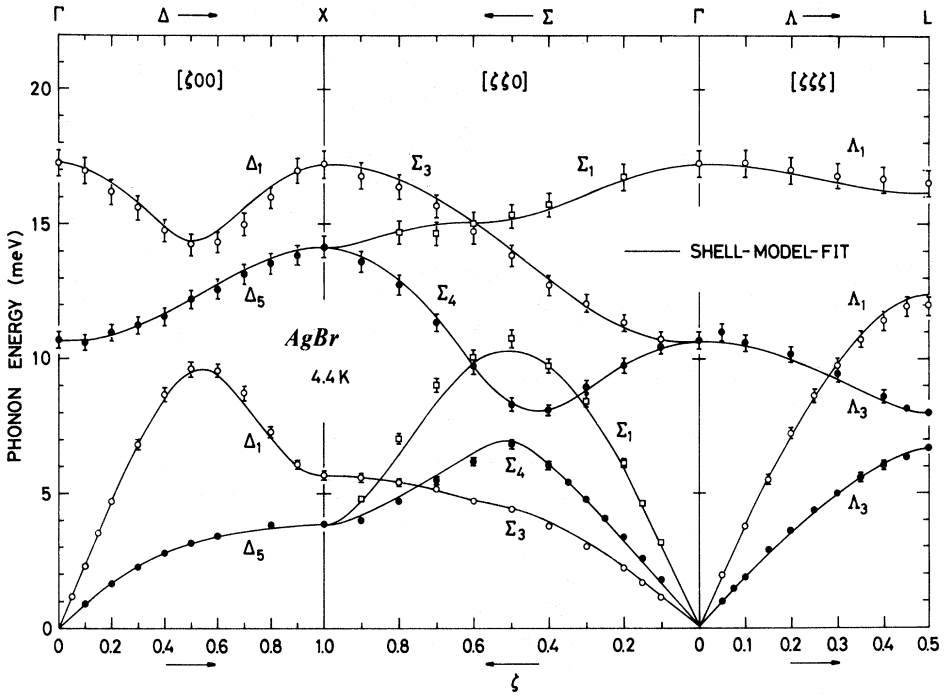

FIG. 2. Observed phonon dispersion relations along the three high-symmetry directions of AgBr at 4.4 K. Solid curves represent an extended-shell-model fit to the data.

tion of 1.0 meV, which is sufficient to clearly resolve the two at the L point. To obtain sufficient counting statistics, we counted 25 min per point. Intensity profiles of the TA and TO phonons observed along the $[\zeta\bar{\zeta}\bar{\zeta}]$ direction through the point $\vec{Q} = (2.5, 1.5, 1.5)$ are displayed in Fig. 3. The solid curves are fitted to the observed values with the method described in Sec. II. From these well-resolved phonon peaks, one can obtain reliable intensity data for these two modes which can then be compared with the shell-model calculation in the next Sec. IV. The phonon energies at L were obtained as follows:

TA (L_3) 6.68 ± 0.10 meV,

TO (L_3) 7.99 ± 0.10 meV,

LA (L_1) 12.00 ± 0.30 meV,

LO (L_1) 16.51 ± 0.50 meV.

The energies of the two momentum conserving phonons participating in the indirect band-gap transition were estimated as 8.0 ± 0.2 and 12.0 ± 0.4 meV at 2 K from optical measurements.[4] The energies of the TO (L_3) and LA (L_1) phonons agree well with these values. It is already known from phonon intensity measurements[9-12] that this assignment satisfies the optical selection rule.

IV. SHELL-MODEL ANALYSIS

A. Phonon dispersion relations

In order to interpret the observed phonon dispersion relation of AgBr, shell-model calculations were carried out. The shell model for the rock-salt structure was developed by Woods *et al.*[14] and Cowley *et al.*[15] for alkali halides. Cochran *et al.*[7] extended it further to analyze their data of PbTe. This model, the so-called "extended-shell model," was also employed for an analysis of the AgCl data and gave a satisfactory fit to the observed phonon dispersion relations.[6] Since then, several modifications of the shell model for silver halides have been made as discussed in Sec. I. In the present analysis, however, the extended-shell model of Cochran *et al.* was utilized simply as a convenient tool to obtain the one-phonon density of states of AgBr.

In the framework of this model under the harmonic, adiabatic, and electrostatic approximations, the equations of motion can be written

$$M\omega^2\vec{U} = (R + ZCZ)\vec{U} + (T + ZCY)\vec{W}, \quad (1)$$

$$0 = (\tilde{T} + YCZ)\vec{U} + (S + YCY)\vec{W}, \quad (2)$$

where R, T, and S are short-range force-constant matrices describing the core-core, core-shell, and shell-shell interactions, respectively. $\tilde{T}$ is the transpose of T. C represents the matrix

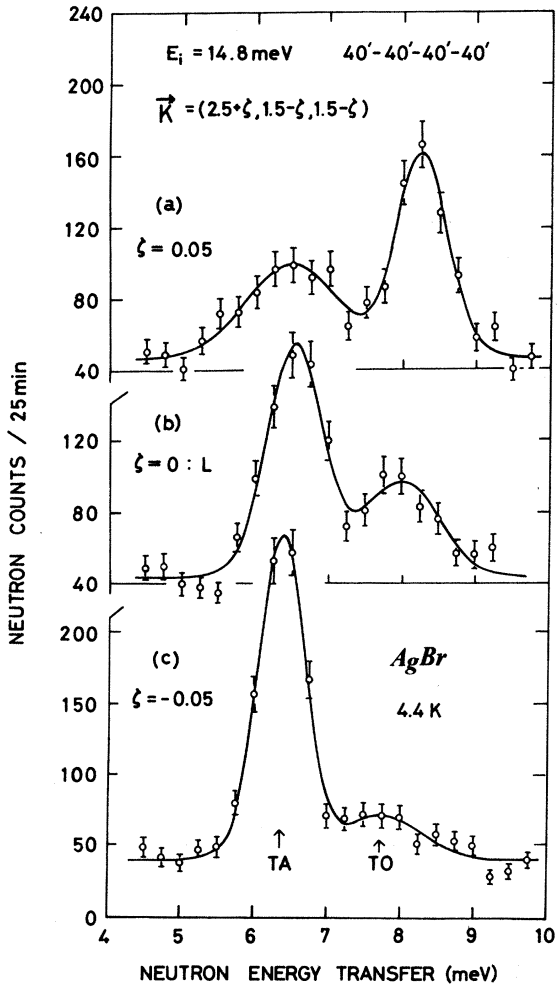

FIG. 3. Phonon scans of the transverse modes along the direction $[\zeta\bar{\zeta}\bar{\zeta}]$ through the L point $\vec{Q}=(2.5, 1.5, 1.5)$ of AgBr at 4.4 K. Solid curves represent a least-squares fit of the sum of two Gaussian functions and a linearly varying background to the data.

of the Coulomb coefficients. M, Z, and Y are diagonal matrices specifying the atomic masses, ionic charges, and shell charges, respectively. $\vec{U}$ and $\vec{W}$ are vectors, with $\vec{U}$ specifying the displacements of the cores while $\vec{W}$ specifies the relative displacements between the cores and their own shells. Thus $Y\vec{W}$ gives the electrostatic dipole moment. For the generalized shell model in which short-range interactions are taken up to the second neighbors, the number of independent parameters is 29. However, this number can be finally reduced to 15 by assuming that the forces are axially symmetric and that the second-neighbor forces act through the shells. The positive ion (Ag) has a core charge $Z|e|$ while the negative one (Br) has the opposite charge, and e is the electronic charge. The short-range force constants for the first neighbor (Ag-Br) are expressed by the parameters A and B which correspond to the radial and tangential forces between the interacting ions, respectively. As for the second-neighbor short-range force constants, A' and B' are used for the Ag-Ag interaction while A'' and B'' are used for the Br-Br one. Electrical (π_i) and mechanical (d_i) polarizabilities ($i=1$ for the positive ion and $i=2$ for the negative one) can be alternately defined in terms of the coupling constant k_i between the core and its own shell and the shell charge $Y_i|e|$ as follows:

$$\pi_i = Y_i^2/(k_i+\alpha)\,, \tag{3}$$

$$d_i = -\alpha Y_i/(k_i+\alpha)\,, \tag{4}$$

where $\alpha = A + 2B$. The other four parameters are concerned with the asymmetry of the first-neighbor core-shell interaction [$\beta_T(12)$, $\beta_T(21)$] and with the shell-shell interaction (α_S, β_S). These notations are discussed more fully in Ref. 7.

The phonon energies and eigenvectors can be calculated from the following equation derived from Eqs. (1) and (2):

$$\{M\omega^2 - [(R+ZCZ) - (T+ZCY)(S+YCY)^{-1}(\tilde{T}+YCZ)]\}\vec{U} = 0\,. \tag{5}$$

Thus calculated energies can be compared with the corresponding observed values and the 15 shell-model parameters iteratively refined. Out of 137 phonon data, 72 data measured at the positions $\vec{q}=(0.2n, 0, 0)$, $(0.2n, 0.2n, 0)$, and $(0.1n, 0.1n, 0.1n)$,

TABLE II. Values of shell-model parameters fitted to AgBr at 4.4 K with those of AgCl previously reported. Short-range force constants are given in units of $e^2/2v$, where v is the volume of the unit cell and e the electronic charge.

	AgBr (4.4 K) Present work	AgCl (78 K) Ref. 6
A	12.02	9.05
B	−3.50	−1.81
A'	−0.431	−0.026
B'	0.081 4	0.025
A''	2.52	2.20
B''	0.187	−0.280
Z	1.09	0.850
π_1	−0.001 32	0.000
d_1	−0.074 0	−0.017
π_2	0.136	0.120
d_2	0.130	0.058
α_S	1.78	1
β_S	−0.724	1
β_T (12)	3.05	4.44
β_T (21)	−0.392	−0.660

TABLE III. Dielectric quantities of AgBr at low temperatures. The energies of the zone-center optical phonons ω_{TO} and ω_{LO} are given in units of meV while the dielectric constants ϵ_0 and ϵ_∞ are dimensionless.

	ω_{TO}	ω_{LO}	ϵ_0	ϵ_∞
Present work				
(a) shell-model fit (4.4 K)	10.64	17.24	10.60	4.04
(b) neutron data (4.4 K)	10.69 ± 0.32	17.24 ± 0.52	···	···
Other experiments				
(c) Lowndes and Martin (2 K)[a]	11.3	···	10.60	4.68
(d) Jones *et al.* (4.2 K)[b]	11.5	···	···	···
(e) Brandt (7.5 K)[c]	···	17.4 ± 0.3	···	···

[a] R. P. Lowndes and D. H. Martin, Proc. R. Soc. A 308, 473 (1969).
[b] G. O. Jones, D. H. Martin, P. A. Mawer, and C. H. Perry, Proc. R. Soc. A 261, 10 (1961).
[c] R. C. Brandt, Appl. Opt. 8, 315 (1969).

with $n = 0 \cdots 5$ were used in the present analysis. The elastic constants (c_{11}, c_{12}, c_{44}) and dielectric constant (ϵ_∞) were also included in the fits.

The best-fit values of parameters are given in Table II together with those for AgCl previously reported.[6] As displayed in Fig. 2, the model fit to the observed phonon dispersion relation is quite satisfactory with the value of χ^2 converging to 1.38. In Tables III and IV, the values of dielectric and elastic quantities calculated from the model are compared with the experimental data. The static dielectric constant ϵ_0 in Table III [row (a)] was obtained by using the Lyddane-Sachs-Teller relation which is rigorously valid in the present model. Also shown in Table IV are values of the bulk modulus $B_0 = \frac{1}{3}(c_{11} + 2c_{12})$, the elastic anisotropy $A = 2c_{44}/(c_{11} - c_{12})$, and a measure, $\delta = (c_{44} - c_{12})/c_{12}$, of the deviation from the Cauchy relation ($c_{44} = c_{12}$).

A calculation of the one-phonon density of states $g(\omega)$ based on the Gilat and Raubenheimer approach[16] was carried out by using the shell-model parameters listed in Table II. The calculation sampled 2340 cubic meshes in the irreducible $\frac{1}{48}$ of the Brillouin zone. The energy channel width was chosen to be 0.02 meV. The results are given in Fig. 4.

B. Mode character at L

A satisfactory lattice-dynamical model for AgBr must first give a satisfactory fit to the observed phonon dispersion relations in order to produce a reliable density of states. It should also be capable of reproducing the eigenvectors of the modes as well. A particularly good test can be made in the present case because of the observed character inversion at the L point. In the Appendix explicit expressions obtained by block diagonalization of the dynamical matrix are given for the eigenenergies and eigenvectors of Eq. (5) at L. We see that at L the Ag and Br atoms vibrate independently of each other. Ordinarily the heavier atom will vibrate with the lower frequency, but this natural tendency can be "inverted" under certain circumstances so that the lighter atom vibrates with the lower frequency, which is the case in AgBr. The transverse phonon energies of Eqs. (A3) and (A4) calculated using the parameters in Table II do show the required character inversion, i.e., $\omega_{1T}(7.99\ \text{meV}) > \omega_{2T}(6.69\ \text{meV})$.

The neutron scattering cross section for the creation of a phonon is

$$\frac{d^2\sigma}{d\Omega\, d\omega} = N \frac{k'}{k} |F_d(\vec{K})|^2 \frac{n_\lambda(\vec{q}) + 1}{\omega_\lambda(\vec{q})}\ , \tag{6}$$

TABLE IV. Elastic quantities of AgBr at low temperatures. The elastic constants c_{ij} and the bulk modulus B_0 are given in units of 10^{11} dyn cm^{-2} while the elastic anisotropy A and the deviation from the Cauchy relation δ are dimensionless.

	c_{11}	c_{12}	c_{44}	B_0	A	δ
(a) Shell-model fit						
Present work (4.4 K)	7.12	3.55	0.851	4.74	0.477	−0.760
(b) Experiments						
Marklund *et al.* (4 K)[a]	6.596[b]	3.494	1.003	4.528	0.647	−0.713

[a] K. Marklund, J. Vallin, and S. A. Mahmoud, Uppsala University Institute of Physics Report No. UUIP-645 (1969) (unpublished).
[b] This value is derived from the observed values of c_{12} and B_0.

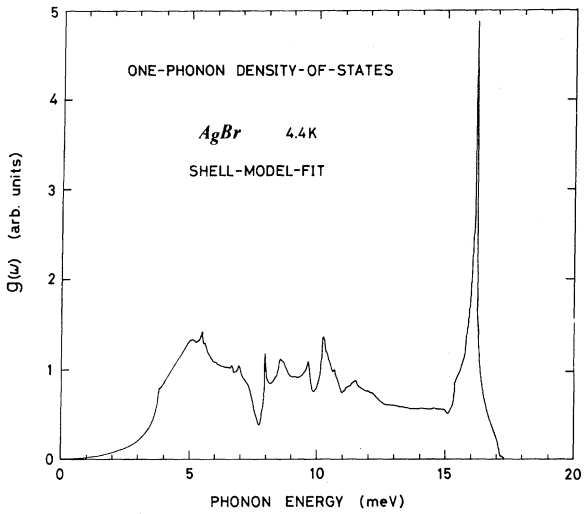

FIG. 4. One-phonon density of states of AgBr at 4.4 K obtained from the extended-shell-model fit.

where the inelastic phonon strucutre factor is given by

$$F_d(\vec{K}) = \sum_j \frac{b_j e^{-W_j(\vec{K})}}{(m_j)^{1/2}} [\vec{K} \cdot \vec{e}_j(\lambda, \vec{q})] e^{i\vec{K}\cdot\vec{r}_j}. \quad (7)$$

N is the number of unit cells contained in a sample, k and k' are the magnitudes of the incident and scattered neutron wave vectors, respectively, $\vec{K}$ is the scattering vector, $W_j(\vec{K})$ the Debye-Waller factor of the jth ion with the mass m_j situated at the position $\vec{r}_j$, and b_j is the coherent neutron scattering length. $\omega_\lambda(\vec{q})$ expresses the phonon energy of the λ branch with the wave vector $\vec{q}$, $n_\lambda(\vec{q})$ is the boson population factor, and $\vec{e}_j(\lambda, \vec{q})$ the eigenvector of the jth ion for the phonon mode specified by λ and $\vec{q}$. The cross section for the TA and TO phonons along the direction $[\zeta\bar{\zeta}\bar{\zeta}]$ through the L point of (2.5, 1.5, 1.5) was calculated by Eq. (6) using the eigenvectors obtained in the present model calculation. $W_j(\vec{K})$ was assumed to be zero for both ions at 4.4 K. The scattering lengths $b_1 = 0.597$ and $b_2 = 0.679$ in units of 10^{-12} cm were used.[17] The experimental values were obtained by integrating the observed intensity in the constant-Q scan as shown in Fig. 3. Figure 5 displays a comparison between the calculation and observation. Both were normalized at the point TA(L) marked with the solid circle. The agreement between them is satisfactory. The intensity ratio of TA to TO modes just at the L point ($\zeta = 0$ in Fig. 5) was calculated to be 2.09 while the observed value was 1.9. If the character inversion did not occur, i.e., the Ag and Br ions are at rest for the TO and TA modes respectively, the ratio is calculated to be 0.67. From these calculations, one can see clear evidence for the character inversion in the transverse mode at the L point.

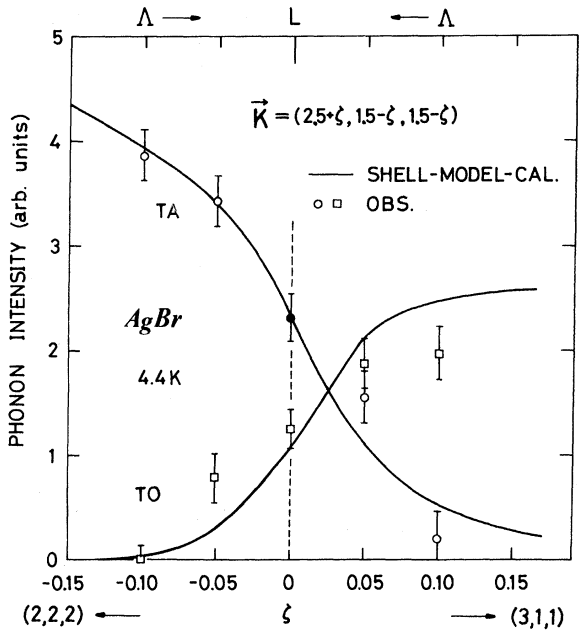

FIG. 5. Phonon intensities of the TA and TO modes along the direction $[\zeta\bar{\zeta}\bar{\zeta}]$ through the L point $\vec{Q} = (2.5, 1.5, 1.5)$ of AgBr at 4.4 K. Solid curves normalized to the observation at TA (L) marked by the solid circles are calculated from the extended shell model. A drastic inversion of intensities can be seen at $\zeta \sim 0.02$, which gives direct evidence for the character inversion between these two modes at the L point.

For the longitudinal mode at the same point, on the other hand, the present calculation shows that only Ag ions contribute to the LA mode while only Br ions to the LO mode. That is, no character inversion occurs in the longitudinal mode.

V. DISCUSSION

A. Lattice-dynamical properties

The present shell-model calculations provide a satisfactory fit to the observed phonon dispersion relation of AgBr at 4.4 K (Fig. 2). However, the final set of parameters (Table II) contain some physically unreasonable quantities such as $\pi_1 < 0$, $\beta_S < 0$, and $\beta_T(21) < 0$. We made various attempts to search for other sets of parameters better than that in Table II, but none were found. Owing to the various assumptions and simplifications used in the model, the values of force-constant parameters may not be expected to have much physical significance. However, this model fit provides a quite satisfactory phenomenological way of fitting and extending our data to calculate the phonon density of states.

TABLE V. Assignments for phonon structures in the optical sideband spectra of AgBr. ΔE: energies of sideband maxima relative to zero-phonon line. Phonon energies: the observed phonon energies corresponding to singularities in the phonon density-of-states spectrum of Fig. 4. For phonons whose mode cannot be assigned, their calculated values are listed with an asterisk.

ΔE (meV)	Phonon energies (meV)	Phonon assignments
	(a) For absorption spectra of Fig. 6	
(3.1)	...	(1s to continuum transition)
7.8	7.99	TO (L)
10.3	10.69	TO (Γ)
	10.78	LA (Σ_1) $\zeta = 0.5$
12.4	12.00	LA (L)?
15.4	15.34*	(LO)
	(b) For luminescence spectra of Fig. 7	
2.1	...	impurity mode due to iodine
4.2	3.87	TA (X)
6.9	6.68	TA (L)
	6.85	TA_1 (Σ_4) $\zeta = 0.5$
8.9	8.56*	...
10.0	10.69	TO (Γ)
	10.78	LA (Σ_1) $\zeta = 0.5$
11.3	11.50*	...
16.8	16.51	LO (L)
	17.24	LO (Γ)

The overall feature of the present one-phonon density of states (Fig. 4) is similar to those obtained from the deformable-shell-model analysis of the 80-K data by Bührer[11] and of the 85-K data by Dorner *et al.*[12] Some phonon energies corresponding to the singular points in the density-of-states spectrum deviate slightly from the observed values. In Table V, the observed phonon energies corresponding to these singularities are listed with their mode assignments for an analysis of optical spectra in the following part.

Together with the previously reported experiments,[9-12] the present high-resolution intensity measurements near the L point confirm the occurrence of the TA-TO character inversion at L. From a lattice-dynamical point of view, such a character inversion is not so unusual in the sense that it often occurs when two phonon branches with the same symmetry approach to each other. One can see a good example in KCl.[18] In the case of AgBr, on the other hand, the mode with the Ag-ion motion is the mode which participates in the momentum conserving phonon participating in the indirect band-gap transition,[4] so that character inversion at L becomes important in discussing the optical selection rule.

In Fischer's model,[8] the shell deformability of the Ag ion has been attributed to causing the character inversion.[10-12] However, the present extended-shell model with rigid shells can also explain it. On the basis of the present model, let's consider the conditions for the occurrence of the character inversion. The energies of the transverse modes are given by Eqs. (A3) and (A4) in the Appendix. The condition for the character inversion is $\omega_{1T} > \omega_{2T}$, i.e.,

$$(1/m_1)(R_{1T} - T_{1T}^2 S_{1T}^{-1}) > (1/m_2)(R_{2T} - T_{2T}^2 S_{2T}^{-1}) . \tag{8}$$

Owing to a large difference between the ionic radii of the Ag and the Br ions, R_{1T} is usually much smaller than R_{2T}. In addition to this, the fact that $m_1 > m_2$ acts against the inequality (8). That is, in the framework of a rigid-ion model in which the terms of $T_{iT}^2 S_{iT}^{-1}$ vanish, the character inversion cannot be produced. In the case of this shell model, the contribution from the $T_{iT}^2 S_{iT}^{-1}$ term is dominant. For the present calculation using the values of force-constant parameters in Table II, the inequality (8) is satisfied. In the silver halides, the character inversion occurs more easily for the Br than the Cl since the Br is heavier. For the longitudinal mode, on the other hand, R_{iL} is found to be the leading term. In this case, the conditions for this character inversion are much more stringent.

B. One-phonon sidebands in the optical spectra

The spectral shape of the one-phonon sidebands associated with the zero-phonon optical transition line corresponds to the spectral density of electron-phonon coupling. As discussed by Toyozawa,[19] the shape of the one-phonon sidebands corresponds closely to the density of states of phonons, in the limit of small orbit radius of the electronic state concerned. This is not the case for AgBr, where the radius of localized electrons is usually much larger than the interatomic distance. For example, the Bohr radius of a simple donor state (electron localized in a Coulomb field) in AgBr is estimated to be 20 Å.[20] When the orbit radius is greater than the lattice constant, coupling with optical phonons will be far greater than that with acoustic phonons, because of the long-range electrostatic interaction associated with the optical mode in contrast with a short-range deformation potential due to the acoustic mode. Furthermore, Toyozawa's theory[19] predicts that the large-radius electron interacts exclusively with the long-wavelength phonons such as the LO(Γ). In the following discussion, two kinds of sideband spectra in AgBr will be discussed and compared with the

one-phonon density of states obtained from the present neutron scattering experiments. The optical spectra to be shown below were remeasured as a part of the present study under the conditions of higher spectral resolution and much lower concentrations of impurities than in the previous experiments.[4,5]

The first spectrum to be discussed is the infrared absorption due to transient shallow donor state in AgBr, first observed by Brandt and Brown.[20] Figure 6 shows the sideband spectra associated with zero-phonon line at 20.8 meV which corresponds to the 1*s* to 2*p* hydrogenic transition. The energy shifts at the sideband maxima are tabulated in Table V(a) and compared with singularities in the one-phonon spectrum of Fig. 4. The 3.1-meV sideband has been assigned to the other electronic transition (1*s* to continuum),[20] consistent with the phonon spectrum. The remaining sidebands can be assigned to the simultaneous emission of lattice phonons with the optical transition. The phonon assignments in Table V(a) suggest the existence of the electron-phonon coupling not only with optical phonons but also with acoustic phonons. The 15.4-meV phonon has the largest coupling strength and is also responsible for the nearly equidistant multiphonon structures in the spectrum in the higher-energy region.[5] The exact nature of the 15.4-meV transition, however, is not yet clear, but may be explained by a final-state interaction such as between the 2*p*-plus-one-LO-phonon and the higher-excited states.

The second example is the luminescence spectrum due to bound exciton at the residual iodine impurity in AgBr. The unique properties of iodine in AgBr was studied in detail by Kanzaki and Sakuragi.[4] Iodine is an efficient hole trap in AgBr and the iodine-bound exciton can be described as an isoelectronic donor state; electron localized in a Coulomb field due to an iodine-bound hole. Figure 7 shows the sideband spectra associated with the zero-phonon line at 2.6412 eV for very low concentration (order of 10^{-6}) of iodine in AgBr. Table V(b) shows the energy shifts at sideband maxima in comparison with singularities in Fig. 4. The 2.1-meV sideband is difficult to be assigned as due to lattice phonon in view of the phonon spectrum. A tentative interpretation for the origin is the quasilocalized impurity mode due to iodine which may be related to the observation of far-infrared absorption due to iodine in AgCl.[21]

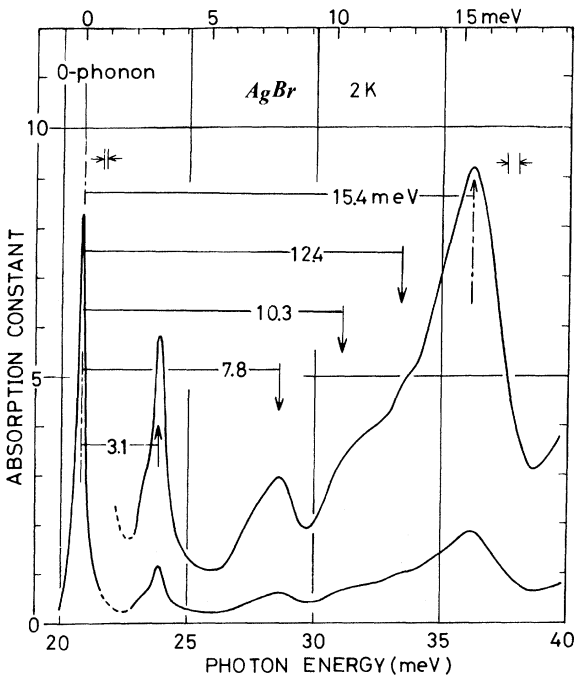

FIG. 6. Optical-absorption spectra due to shallow donor center in AgBr during uv excitation at 2 K. The zero-phonon line is located at 20.8 meV. The upper curve is drawn with expanded scale to show the details of the sidebands. Absorption constant is in arbitrary units.

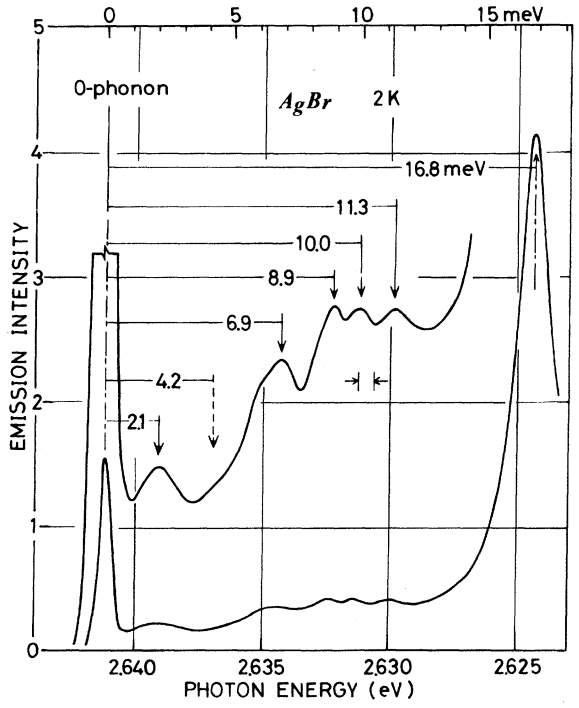

FIG. 7. Photoluminescence spectra due to residual iodine impurity (concentration of the order of 10^{-6}) in AgBr at 2 K. The zero-phonon line is located at 2.6412 eV. The upper curve is drawn with expanded scale to show the details of the sidebands. Emission intensity is in arbitrary units.

This point requires further investigations. The most strongly coupled phonon of 16.8 meV is also responsible for the multiphonon structures studied previously[4] and can be identified as the LO(Γ) as expected theoretically. On the other hand, it is seen that various acoustic phonons also contribute to the phonon sidebands in addition to optical phonons. This can be explained, at least qualitatively, by a coupling of phonons with the localized hole at the iodine site having a smaller orbit radius compared with an electron in a Coulomb field.[4] This feature in the electron-phonon coupling is also related to the different values of coupling strength S between spectra of Fig. 6 ($S \approx 2$) and of Fig. 7 ($S \approx 6$) obtained from the multiphonon structures.[4,5]

To sum up, the one-phonon sidebands in the optical spectra of AgBr have been analyzed in terms of the one-phonon density of states determined from the neutron scattering experiments. Although some of the quantitative features require further studies, several qualitative conclusions can be drawn. One is the discrimination of phonon sidebands due to lattice phonons from those of other origins, such as that due to other electronic transition (3.1-meV band in Fig. 6). The other is the difference in the electron-phonon coupling between electronic states with different characters, such as between electrons in shallow donor states and holes in deep-localized state constituting localized excitons. Further discussions on the optical transitions treated here will be given elsewhere.

ACKNOWLEDGMENTS

The authors wish to thank Dr. N. Wakabayashi and Dr. R. M. Nicklow of the Oak Ridge National Laboratory for providing the computing programs of the shell-model calculations and density of states. The calculations were performed with both computers FACOM 230-48 and HITAC 8800 installed at the Institute for Solid State Physics and The Computer Center of The University of Tokyo respectively. Discussions on phonon sidebands with Professor Y. Toyozawa of the Institute for Solid State Physics, The University of Tokyo are also appreciated.

APPENDIX

Owing to the symmetry of the L point, $\vec{q} = (\frac{1}{2}, \frac{1}{2}, \frac{1}{2})$, of the rocksalt-type structure, Eq. (5) can be block diagonalized as follows:

$$\begin{pmatrix} D_{1T}-\omega^2 & 0 & 0 & 0 & 0 & 0 \\ 0 & D_{2T}-\omega^2 & 0 & 0 & 0 & 0 \\ 0 & 0 & D_{1T}-\omega^2 & 0 & 0 & 0 \\ 0 & 0 & 0 & D_{2T}-\omega^2 & 0 & 0 \\ 0 & 0 & 0 & 0 & D_{1L}-\omega^2 & 0 \\ 0 & 0 & 0 & 0 & 0 & D_{2L}-\omega^2 \end{pmatrix} \begin{pmatrix} U_{1x}-U_{1y} \\ U_{2x}-U_{2y} \\ U_{1x}+U_{1y}-2U_{1z} \\ U_{2x}+U_{2y}-2U_{2z} \\ U_{1x}+U_{1y}+U_{1z} \\ U_{2x}+U_{2y}+U_{2z} \end{pmatrix} = 0 , \tag{A1}$$

where

$$D_{i\lambda} = (e^2/2v)(1/m_i)(R_{i\lambda} - T_{i\lambda}^2 S_{i\lambda}^{-1}) . \tag{A2}$$

This expression can be obtained independent of models. For the extended shell model, the elements of the dynamical matrix in Eq. (A2) are given by

$$R_{i\lambda} = (\alpha + \beta_{i\lambda}) + C_\lambda Z_i^2 ,$$

$$T_{i\lambda} = (\alpha + \beta_{i\lambda}) + C_\lambda Z_i Y_i ,$$

$$S_{i\lambda} = (\alpha + \beta_{i\lambda}) + k_i + C_\lambda Y_i^2 .$$

The suffix i specifies the ion (1, Ag; 2, Br) and λ the phonon mode (T, transverse; L, longitudinal). C_λ is the Coulomb coefficient; $C_L = -2C_T = 7.230\,30$. Z_i is the core charge; $Z_1 = -Z_2 = Z$. $\beta_{i\lambda}$ expresses the second-neighbor interactions; $\beta_{1T} = A' + 5B'$, $\beta_{2T} = A'' + 5B''$, $\beta_{1L} = 4A' + 2B'$, and $\beta_{2L} = 4A'' + 2B''$. As can be seen in Eq. (A1), only one ion, Ag or Br, vibrates for each type of phonon mode; the transverse modes are doubly degenerate. The energies of the transverse modes are then

$$\omega_{1T}^2 = (e^2/2v)(1/m_1)(R_{1T} - T_{1T}^2 S_{1T}^{-1}) \quad \text{for Ag} , \tag{A3}$$

$$\omega_{2T}^2 = (e^2/2v)(1/m_2)(R_{2T} - T_{2T}^2 S_{2T}^{-1}) \quad \text{for Br} . \tag{A4}$$

*Present address: Dept. of Physics, University of Maryland, College Park, Md. 20742.

†Work performed under the auspices of the U. S. Energy Research and Development Administration.

[1] For a review see, F. C. Brown, in *Solid State Chemistry*, edited by B. Hannay (Plenum, New York, 1975).

[2] F. Bassani, R. S. Knox, and W. B. Fowler, Phys. Rev. 137, A1217 (1965); P. M. Scop, Phys. Rev. 139, A934

(1965).
[3]H. Tamura and T. Masumi, Solid State Commun. 12, 1183 (1973).
[4]H. Kanzaki and S. Sakuragi, J. Phys. Soc. Jpn. 27, 109 (1969); 29, 924 (1970); 29, 936 (1970).
[5]H. Kanzaki and S. Sakuragi, Solid State Commun. 9, 1667 (1971); Photogr. Sci. Eng. 17, 69 (1973).
[6]P. R. Vijayaraghavan, R. M. Nicklow, H. G. Smith, and M. K. Wilkinson, Phys. Rev. B 1, 4819 (1970).
[7]W. Cochran, R. A. Cowley, G. Dolling, and M. M. Elcombe, Proc. R. Soc. A 293, 433 (1966).
[8]K. Fischer, H. Bilz, R. Haberkorn, and W. Weber, Phys. Status Solidi B 54, 285 (1972).
[9]H. Kanzaki, S. Sakuragi, S. Hoshino, G. Shirane, and Y. Fujii, Solid State Commun. 15, 1547 (1974).
[10]W. von der Osten and B. Dorner, Solid State Commun. 16, 431 (1975).
[11]W. Bührer, Phys. Status Solidi B 68, 739 (1975).
[12]B. Dorner, W. von der Osten, and W. Bührer, J. Phys. C 9, 723 (1976).
[13]R. P. Lowndes, Phys. Rev. B 6, 1490 (1972).
[14]A. D. B. Woods, W. Cochran and B. N. Brockhouse, Phys. Rev. 119, 980 (1960).
[15]R. A. Cowley, W. Cochran, B. N. Brockhouse, and A. D. B. Woods, Phys. Rev. 131, 1030 (1963).
[16]G. Gilat and L. J. Raubenheimer, Phys. Rev. 144, 390 (1966).
[17]C. G. Shull (private communication); G. E. Bacon, Acta Crystallogr. A 28, 357 (1972).
[18]J. R. D. Copley, R. W. Macpherson, and T. Timusk, Phys. Rev. 182, 965 (1969).
[19]Y. Toyozawa, in *Dynamical Processes in Solid State Optics*, edited by R. Kubo and H. Kamimura (Benjamin, New York, 1967).
[20]R. C. Brandt and F. C. Brown, Phys. Rev. 181, 1241 (1969).
[21]C. K. Chau and M. V. Klein, Phys. Rev. B 1, 2642 (1970).